THE ASTROPHYSICAL JOURNAL, 248:684–695, 1981 September 1

TIME-RESOLVED SPECTROSCOPY OF CATACLYSMIC VARIABLES: U GEMINORUM

R. J. STOVER[1]
McDonald Observatory; and Department of Astronomy, University of Texas at Austin
Received 1980 December 11; accepted 1981 March 18

ABSTRACT

Spectroscopic observations of the dwarf nova U Gem are presented. We also present new measurements of the radial-velocity variations of the accretion disk emission lines. With these new measurements, we derive the masses of the white dwarf primary and the red dwarf secondary: $M_{wd} = 1.18\ M_{\odot}$, $M_{red} = 0.56\ M_{\odot}$. Analysis of the emission-line profiles show that the disk in U Gem cannot be approximated by a model in which the disk particles are assumed to follow simple periodic orbits described by the three-body approximation. Furthermore, the line profiles indicate the presence of turbulent velocities in the disk.

Subject headings: stars: accretion — stars: dwarf novae — stars: individual — stars: U Geminorum

I. INTRODUCTION

The eclipsing binary U Gem is the prototype of the dwarf nova class of cataclysmic variables. The photometric study of U Gem by Krzeminski (1965) showed that U Gem is an eclipsing binary system with an orbital period of 4^h15^m. Later photometric studies of U Gem by Warner and Nather (1971) and Smak (1971) led to a model whose basic properties are believed to apply to many cataclysmic variables and almost certainly to all dwarf novae. The model includes a close binary system in which the degenerate primary star is surrounded by a gaseous ring or disk. The material for the disk is supplied by mass exchange from the dwarf secondary star through the inner Lagrangian point. This accretion stream encounters the outer edge of the disk, producing a shock front, normally referred to as the bright spot because it is a major source of luminosity for the system. The complex interactions between the binary components, the stream of transferring material and the disk, along with the binary's orbital motion and inclination, are believed to account for most of the observed properties of dwarf novae. In U Gem the observed eclipse is an eclipse of the bright spot by the mass-losing secondary star.

The excellent spectroscopic radial-velocity study of U Gem by Smak (1976) provided the first measurements of the system's basic physical parameters. In U Gem there is a region of enhanced emission close to the bright spot where the stream of transferring material impacts the outer edge of the disk. This enhanced emission is normally referred to as the "S-wave" component because of its characteristic appearance on single-trailed photographic spectra. Smak (1976) showed that the S-wave component of the emission lines contributes significantly to the line emission coming from the disk and can seriously distort the observed radial velocities. He also showed that, within the three-body approximation, particle trajectories in the outer portion of the disk may depart significantly from Keplerian motions and that these departures may seriously affect the radial velocities measured.

Smak (1976) was able to overcome the first complication by carefully eliminating from the analysis the radial-velocity measurements contaminated by the S-wave. The second complication, however, required interpretation of the data within a specific disk model. The Smak (1976) model assumes that the rotation of the disk can be approximated by the periodic solutions of the three-body problem, that the S-wave arises in the accretion stream and not in the impact spot, that the peaks of the emission lines arise from material following some particular, though unspecified, particle trajectory within the disk, and that the impact spot has no effect on the structure of the outer portions of the disk. Though Smak's (1976) derived orbital and physical parameters appear reasonable, such modeling can lead to systematic errors in the final radial velocities and in the system's derived physical state.

Because U Gem is of such fundamental importance to the study and understanding of cataclysmic variables, we have obtained a new series of time-resolved spectroscopic observations of U Gem at minimum light. The data were obtained with the Cassegrain Digicon Spectrograph (CDS) on the McDonald Observatory 2.1 m Struve reflector. Using these data, we have measured the emission-line radial velocities in a manner which minimizes the effect of the complications encountered by Smak (1976). We have also investigated the emission-line profiles for clues to the structure of the accretion disk and, in so doing, have examined several of the assumptions used by Smak (1976) in his analysis. Finally, we have attempted to separate the S-wave component from the double-line emission component in order to get a better measurement of its radial-velocity variations.

[1] Now at Lick Observatory.

II. OBSERVATIONS

Fourty-four spectroscopic observations of U Gem were obtained on the nights of 1978 December 19–December 22 UT using the CDS. Because the CDS employs a dual, 936 element, diode array Digicon detector, each observation results in two time-interlaced, sky-subtracted spectra. Details of the CDS are given by Tull, Vogt, and Kelton (1979), and a complete description of our observing techniques and reduction procedures is given by Stover *et al.* (1980, Paper I). The results of Paper I showed that the CDS is a highly stable instrument capable of being accurately calibrated in wavelength and is therefore able to obtain data suitable for accurate radial-velocity measurements. Because our primary objective was to obtain the best possible wavelength calibration for radial-velocity studies, we used a narrow (1″.2) spectrograph entrance slit. Therefore, our data cannot be used to obtain absolute line strengths though relative line strengths are good to 10–15%. The present spectra, each with a 20 minute total exposure, cover a useful wavelength range from 3600 Å to 5100 Å at a dispersion of approximately 1.9 Å per pixel and a resolution of 3.8 Å. Each observation of U Gem was bracketed by observations of argon and neon emission lamps for wavelength calibration. In addition to the U Gem spectra, a tungsten-filament lamp and the flux standard HR 4694 were observed through a wide entrance slit in order to determine the instrument response. As described in Paper I, all U Gem observations were reduced to relative fluxes, f_ν, and transformed onto a linear wavelength scale. For all measurements presented in this paper, the two spectra obtained during each observation were first co-added to increase the signal-to-noise ratio.

Figure 1 shows the time-averaged appearance of the visual spectrum of U Gem formed by co-adding all 44 observations in the rest frame of the white dwarf. The broad, doubled emission lines arise from the rotating disk of gas surrounding the white dwarf. The strongest lines are those of hydrogen and calcium, with much weaker lines of helium. The full width of the Balmer lines is 5000 km s^{-1}, and the double peaks are separated by 1130 km s^{-1}. The region between 4470 Å and about 4700 Å appears to be in continuous emission and may be the blend of many weak features. No absorption lines from either the secondary or primary stars can be seen in this region of the spectrum.

Not obvious in Figure 1 is the effect of the S-wave. Because it arises in the bright impact spot at the edge of the disk or in the accretion stream just in front of the spot, the S-wave appears as a single, relatively narrow line which moves back and forth across the double-line disk component. However, the apparent intensity of the S-wave is not constant with orbital phase and, in the time-averaged plot, causes the red wing of the Balmer lines to appear stronger than the blue wing. In addition, the He I lines at 4922 Å and 5016 Å arise largely, though not entirely, from the S-wave; the doubling of the lines in Figure 1 mostly reflects the time-averaged intensity of the spot emission. The effect of the eclipse on the appearance of the spectrum cannot be shown because none of our spectra were centered on the time of mid-eclipse. In addition, none of our spectra show the typical eclipse disturbance in the emission-line profiles which would be expected if an appreciable fraction of the disk were eclipsed.

III. ANALYSIS

a) Phase Bin Spectra

In Figure 2 the 44 U Gem spectra have been summed into 10 nonoverlapping orbital phase bins. Before co-adding the spectra, the Doppler shift of the emission lines due to the apparent orbital motion has been removed from the data. Phase 0.0 corresponds to the phase of maximum positive radial velocity of the double-line component. The phases shown in all other figures in this paper are also defined in the same way. The resulting 10 spectra have been scaled to maintain a constant continuum value, although, in absolute units, the continuum becomes much brighter just before the eclipse at spectroscopic phase 0.25. The unfiltered photometry shown in Figure 3 illustrates the typical changes in the continuum as a function of orbital phase. The data used to produce Figure 3 are the same data used in Figure 2 of Warner and Nather (1971).

The most striking, phase-related change visible in the time-resolved spectra is the movement of the S-wave back and forth across the double-line component. At phases 0.0 and 0.1, just before the eclipse, the continuum is very strong and the emission lines appear relatively weak. In fact, at these phases, there may be a central absorption component in the Balmer lines. At phase 0.2, near the peak of the photometric "hump," the central absorption is particularly obvious in Hγ and even more so in Hδ which appears to drop below the local continuum at the line center. By phase 0.3, the eclipse has occurred, the continuum is much weaker, and the relative strength of the Balmer lines has increased. At this phase, the S-wave is just to the right (longward) of line center, and the double component is relatively uncontaminated, with a V/R ratio near unity. By phase 0.5, the S-wave has moved to its extreme longward position and has also increased in relative strength, indicating that the region of emission appears brighter when the bright spot is roughly on the far side of the disk. The S-wave has moved back toward line center by phase 0.7 but still remains relatively strong. In particular, it appears much stronger than when it was near line center at phase 0.2.

The phase-related changes in the weak He I lines at 4922 Å and 5016 Å are very apparent because these lines arise mostly, but not entirely, from the S-wave component. The strengthening of the S-wave at about phase 0.4 also occurs in the helium lines. The He I triplet lines at 4024 Å and 4471 Å, which appear strongly in SS Cygni (Paper I), do not appear strongly in U Gem, even in the S-wave. Suppression of these lines below the intensities of the He I singlets at 4922 Å and 5016 Å requires very high densities ($n_e \gg 10^7$ cm^{-3}) and optical depths within the lines ($\tau \gg 100$). Theoretical He I-line strength calculations at such physical conditions have not yet been done.

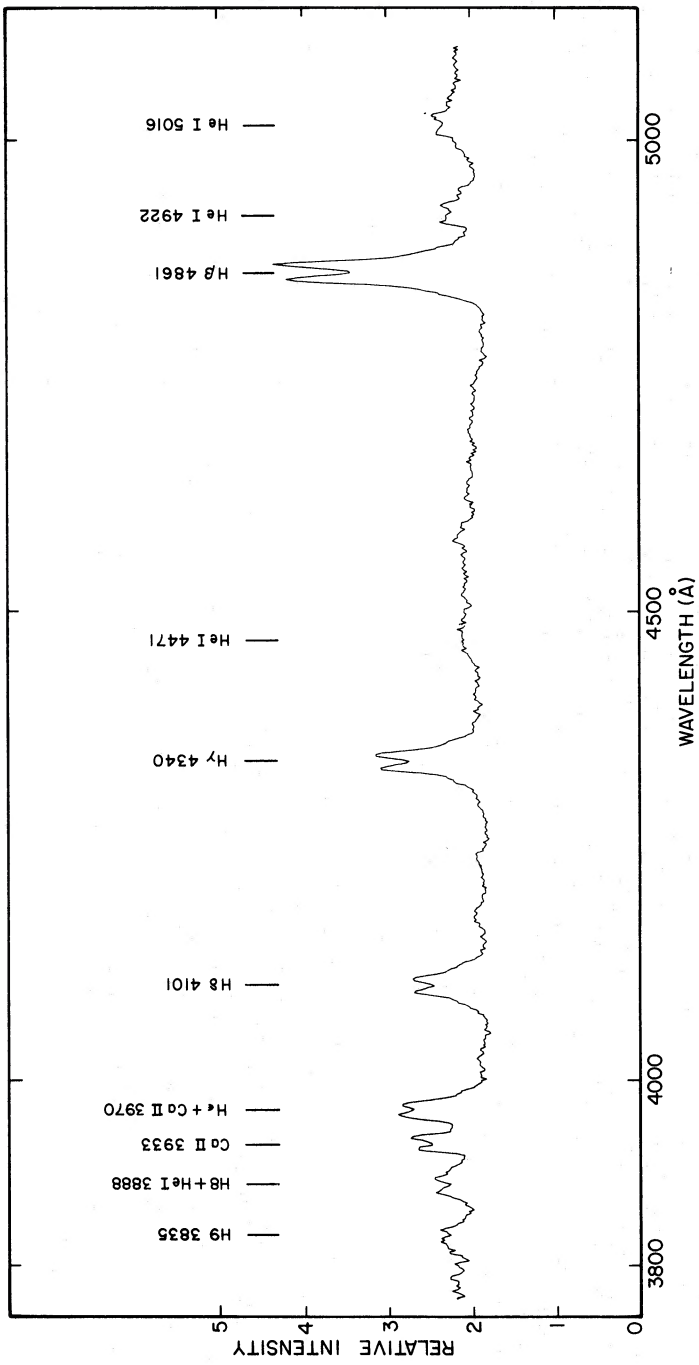

FIG. 1.—Average spectrum of U Gem. This spectrum was formed by co-addition of 44 individual spectra in the rest frame of the emission lines

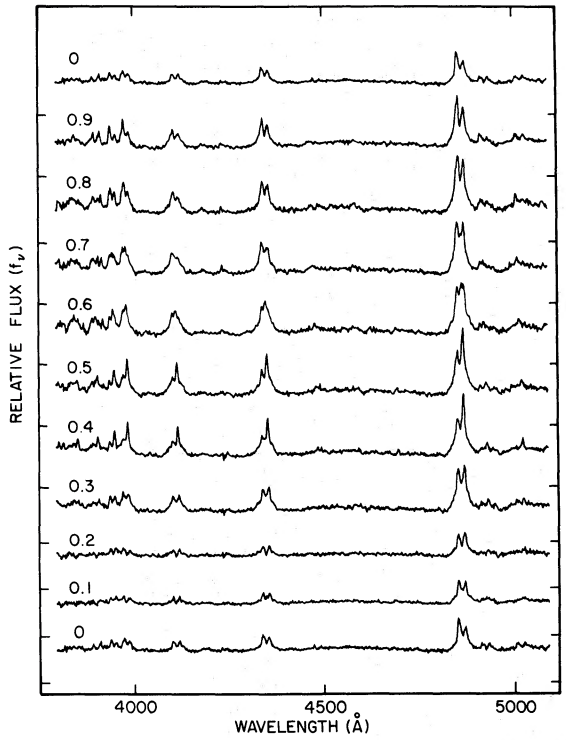

FIG. 2.—Phase bin spectra. The 44 individual spectra are co-added into 10 nonoverlapping orbital phase bins. The zero-intensity level is indicated for each spectrum.

The Ca II line at 3933 Å goes through changes similar to the Balmer lines, although the strength of the S-wave relative to the double component is slightly greater.

b) *Disk Radial Velocities*

As was done in the analysis of SS Cygni (Paper I), the positions of the Balmer lines Hβ, Hγ, and Hδ were measured by fitting a low-order symmetric polynomial to the wings of the profiles. The central regions of each component of the double-line profile are periodically blended with the S-wave because they both arise from low-velocity material near the outer edge of the disk. In addition, this is the very material most likely to show non-Keplerian motions. However, by measuring the position of the wings, we have minimized both of these complications.

In Table 1 we present the measured heliocentric radial velocities. The second column gives the mean heliocentric Julian Date for each observation. Although the last column gives the measured radial velocities for Hδ, we have not included them in the analysis of the orbital parameters because Hδ is apparently blended with He I 4121 Å. In Figure 4 we plot the average radial velocities for Hβ and Hγ given in Table 1 folded on the orbital period. The solid curve represents the circular orbit solution whose parameters are given in Table 2. We have also included in Table 2 the individual orbital solutions for Hβ, Hγ, and Hδ. As can be seen in Table 2, all three lines give consistent K velocities, although the gamma velocity of Hδ is seriously affected by the blend.

c) S-*wave Radial Velocities*

Radial-velocity measurements of the disk emission lines in U Gem, and in many other cataclysmic variables, are complicated by the presence of the additional S-wave emission line. In order to measure the radial-velocity variations of the S-wave when it is blended with one of the components of the double-line profile, one is forced to make some assumptions about the nature of the emission lines. The basic assumption we have made in extracting the S-wave is that the double component is symmetric. Because the S-wave may form a blend with either the red wing or the blue wing but never with both, our assumption allows us to use the unblended component to define the shape of the underlying blended component. One complication arises in trying to define the central intensity of the double component. Consider, for instance, phase 0.7 in Figure 2, where the S-wave, if present, lies close to the line center. Here the double component

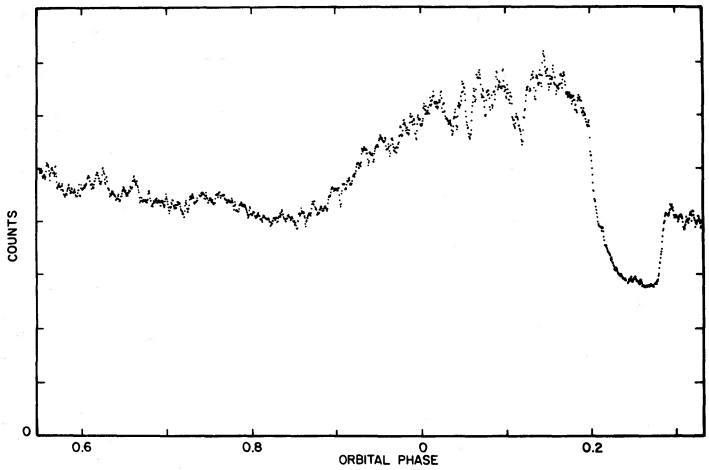

FIG. 3.—Unfiltered photometry of U Gem. Each point represents an integration of 4 s in unfiltered light

TABLE 1

U GEMINORUM DISK RADIAL VELOCITIES

No.	DATE (JD$_\odot$ 2443860+)	RADIAL VELOCITY (km s^{-1}) Hβ	Hγ	Hδ
1	1.79856	135	154	79
2	1.81453	94	107	160
3	1.83050	174	162	222
4	1.84648	143	44	-229
5	1.86245	-29	36	259
6	1.87842	-23	-66	68
7	2.77102	-146	-84	71
8	2.78699	-192	-195	-21
9	2.80296	-101	-106	-43
10	2.81893	-55	50	-31
11	2.83490	33	79	75
12	2.85088	133	97	66
13	2.86685	237	199	215
14	3.77152	142	-106	185
15	3.78922	87	36	75
16	3.80519	-52	-67	66
17	3.82117	-21	-15	-166
18	3.83714	-70	-144	-81
19	3.85311	-118	-207	106
20	3.86908	-87	45	-134
21	3.88505	1	-86	-31
22	3.90103	72	109	30
23	3.91700	89	18	166
24	3.93297	124	118	264
25	3.94894	92	168	107
26	3.96491	77	44	199
27	3.98089	-10	-32	139
28	3.99686	-130	-44	-64
29	4.01381	-80	-168	-130
30	4.74853	-89	-151	-72
31	4.76451	-28	-154	-79
32	4.78048	82	39	-10
33	4.80134	123	96	246
34	4.81731	139	150	191
35	4.83328	145	160	63
36	4.84925	25	98	16
37	4.86522	15	18	-35
38	4.88119	2	-15	7
39	4.89717	-105	-81	-117
40	4.91314	-211	-166	-202
41	4.92911	-79	-65	-119
42	4.94508	-25	-29	18
43	4.96105	77	73	136
44	4.97702	90	113	254

appears to be symmetric, but it is not obvious whether the observed central intensity is the intrinsic intensity of the double component or whether it is a result of a blend with the S-wave. In such cases, we have adopted the central intensity to be 50% of the intensity of the unblended emission peaks. When the S-wave is located at its extreme red or blue positions, blending with the center of the double component is not important. At these phases, the measured central intensity is also roughly 50 to 70%.

Figure 5 shows the results of removing the (assumed) symmetric Hβ double-lined profile. As in Figure 2, all of the data have been summed into 10 orbital phase intervals with the apparent orbital motion removed. For each phase interval, both the original profile and the extracted S-wave are shown. Some smearing of the S-wave profile has occurred because of the finite width of the phase

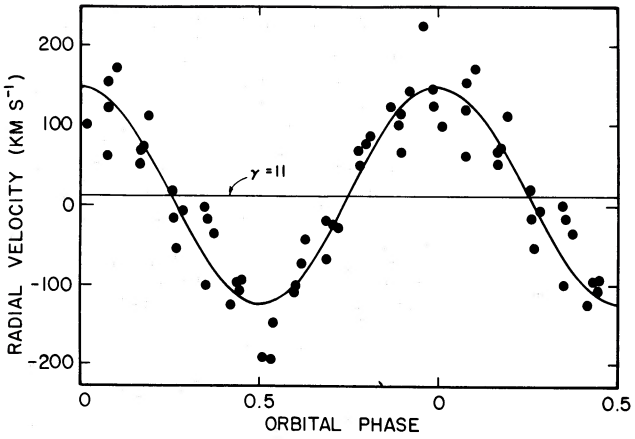

FIG. 4.—Average measured radial velocities of Hβ and Hγ. The solid curve represents the circular orbit solution in Table 2.

intervals. The analysis shows that the S-wave, when visible, is relatively narrow with a full width of 6.5 Å. Furthermore, there are no broad wings, thus ensuring that our disk radial velocities are free from contaminating effects of the S-wave. Because the S-wave appears to have a simple shape, the radial-velocity variations were measured by fitting a simple parabola to the peak of the S-wave profile. However, between phases 0.05 and 0.35, the S-wave is essentially absent and therefore radial velocities could not be measured. The results of the radial-velocity measurements of Hβ and Hγ are given in Table 3 and shown in Figure 6, plotted against orbital phase as deduced from the disk radial velocities. The derived parameters of a sinusoidal fit to the velocity measurements are given in Table 2. Because Hδ is much weaker than Hγ, the low signal-to-noise ratio in the individual spectra make the extraction of the Hδ S-wave very uncertain and the resulting radial velocities highly inaccurate.

TABLE 2

RADIAL-VELOCITY PARAMETERS
($P = 0^d.176906$, $e = 0$ assumed)

Line[a]	K (km s^{-1})	γ (km s^{-1})	T_{max}[b] (JD$_\odot$ 2443860+)
Disk			
Hβ (2)	138 ± 9	14 ± 6	1.8125 ± 0.0018
Hγ (1)	137 ± 12	10 ± 8	1.8127 ± 0.0024
Hδ (0)	133 ± 18	52 ± 13	1.8179 ± 0.0038
Avg.	137 ± 8	11 ± 6	1.8122 ± 0.0016
S-Wave			
Hβ (2)	408 ± 20	97 ± 18	1.8782 ± 0.0019
Hγ (1)	490 ± 34	81 ± 27	1.8702 ± 0.0023
Avg.	432 ± 17	92 ± 14	1.8752 ± 0.0014

[a] Numbers in parenthesis indicate weighting factors used to form the average.

[b] T_{max} is the time of maximum positive velocity.

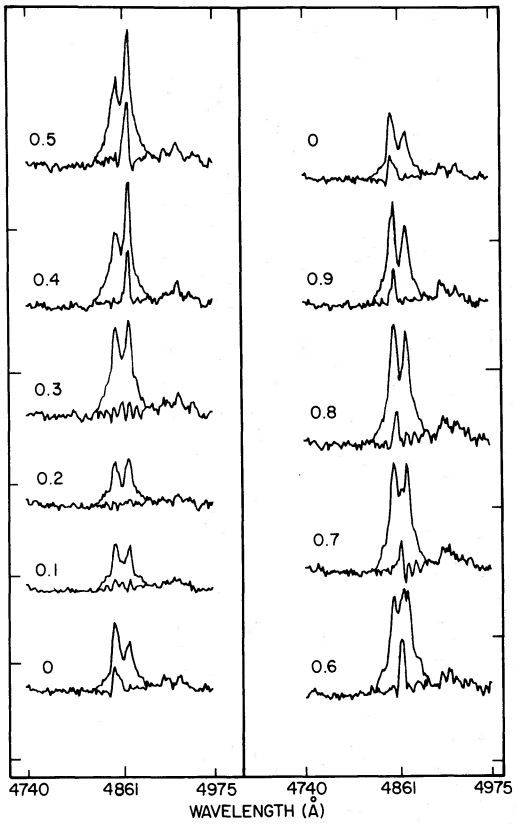

FIG. 5.—S-wave extraction from Hβ. The extracted S-wave is shown in 10 orbital phase bins. The zero-intensity level is indicated for each spectrum.

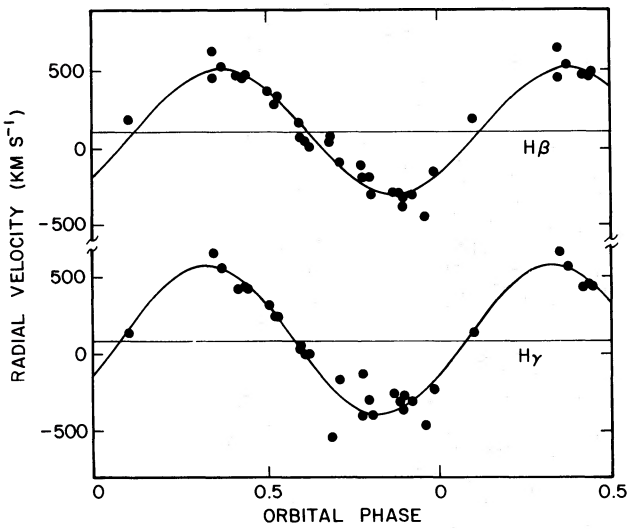

FIG. 6.—Measured radial velocities of the S-wave extracted from Hβ and Hγ. The solid curves represent the sinusoidal solutions in Table 2.

TABLE 3

U GEMINORUM S-WAVE RADIAL VELOCITIES

No.	DATE ($JD_\odot$ 2443860+)	R.V. (km s^{-1}) Hβ	Hγ
1	1.79856	−320	−313
2	1.83050	174	128
3	1.87842	520	557
4	2.77102	463	420
5	2.78699	362	309
6	2.80296	57	45
7	2.81893	57	−552
8	2.83490	−205	−140
9	2.85088	−305	−270
10	2.86685	−464	−477
11	3.83714	457	422
12	3.85311	329	233
13	3.86908	0	−1
14	3.88505	−105	−178
15	3.90103	−312	−401
16	3.91700	−328	−373
17	3.99686	444	650
18	4.01381	474	429
19	4.74853	156	24
20	4.76451	31	−544
21	4.78048	−121	−407
22	4.80134	−390	−289
23	4.81731	−172	−239
24	4.88119	625	644
25	4.89717	449	437
26	4.91314	269	233
27	4.92911	32	−5
28	4.96105	−207	−314
29	4.97702	−304	−321

d) Peak Velocities

Simple model calculations of the profiles of emission lines arising from a disk (Smak 1970; Huang 1972) have shown that the peaks of the observed double profiles correspond to the rotational velocity at the outer edge of the disk. Smak (1976) employs this property in his model used for the analysis of U Gem. In addition, Smak (1976) assumes that the disk is pressure free so that the material in the disk follows simple periodic orbits allowed within the three-body approximation. Paczynski (1977) computed a series of pressure-free disk models identical to those used by Smak (1976) and showed that, since the outermost orbits are very noncircular and the velocities are position-angle dependent, the observed disk rotation velocity should vary as a function of orbital phase. For U Gem, the full amplitude of the variation is predicted to be 125 km s^{-1}.

To measure the variation of the emission-peak velocities, we first transformed our spectra to remove the apparent orbital motion measured from the wings. The positions of both the red and blue peaks were then measured by fitting a low-order polynomial. The average velocities for Hβ, Hγ, and Hδ are shown in Figure 7. The solid line represents the mean radial-velocity curve found for the S-wave component. Except for the obvious disturbance by the S-wave, no radial-velocity variations

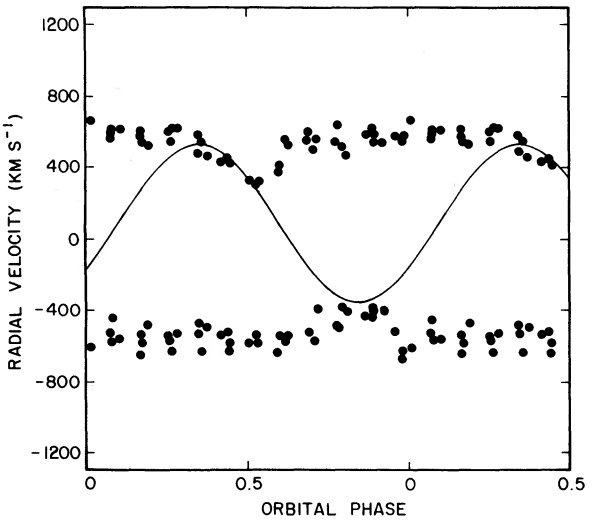

FIG. 7.—Average measured radial velocities of the emission-line peaks. The solid curve represents the mean radial-velocity curve of the S-wave.

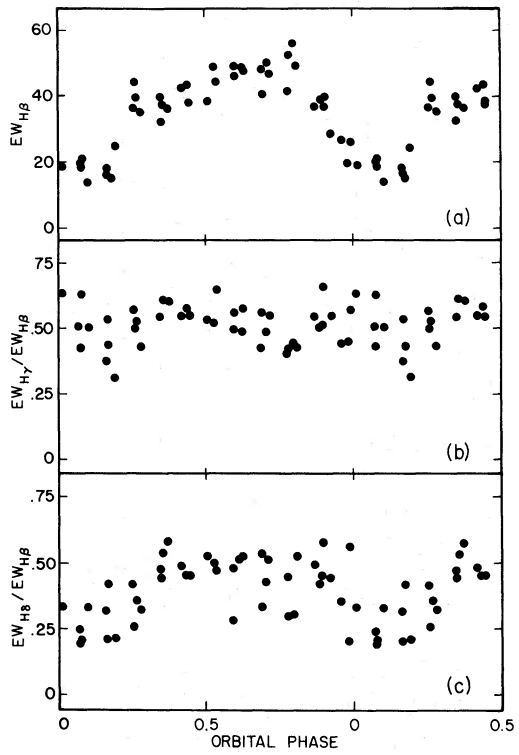

FIG. 8.—Emission-line equivalent widths as a function of orbital phase: (*a*) shows the measured equivalent widths of Hβ; (*b*) and (*c*) show, respectively, the Hγ and Hδ equivalent widths relative to those of Hβ.

are apparent, with an upper limit to the full amplitude of about 40 km s^{-1}. Because the expected velocity variations would repeat with a period of half the orbital period, one cannot explain the apparent absence of variation as improper removal of the orbital motion or as masking by the S-wave disturbance which both repeat at the orbital period. The mean projected rotational velocity defined by half the peak separation is 564 ± 20 km s^{-1}. No significant differences in the rotational velocity were found among the three Balmer lines except for the red wing of Hδ, which was about 60 km s^{-1} greater than all of the other measurements because of the blend with He I 4121 Å. From this analysis, we conclude that simple, pressure-free disk models do not describe accurately the motion of particles in the disk of U Gem and that they overestimate the variation in peak separation by at least a factor of 3.

e) Equivalent Widths

Under ideal circumstances, the equivalent widths of the emission lines would provide information on the physical conditions within the accretion disk. However, the circumstances are far from ideal, and the interpretation of the equivalent widths is complicated by several factors. First, the continuum intensity varies by at least a factor of 2 during each orbit because of the varying visibility of the bright spot. Second, the observed emission lines arise from at least three separate, possibly varying components: the disk emission, the S-wave emission, and the central absorption. Furthermore, the disk emission represents an integration over the entire disk, which can encompass a wide range of physical conditions. Nevertheless, the equivalent widths can be used in a straightforward manner to detect relative changes between the lines.

The upper portion of Figure 8 illustrates the large changes in the measured Hβ equivalent width as a function of orbital phase. Compared to the light-curve shown in Figure 3, the Hβ equivalent widths exhibit an almost identical but inverted orbital variation, showing that continuum changes are the predominant cause of the equivalent-width variations. Although there are large orbital modulations, we find no systematic variations from one day to the next at a fixed orbital phase. The lower sections of Figure 8 show the equivalent widths of Hγ and Hδ relative to Hβ. The variations in Hγ match fairly closely the changes in Hβ, while the changes in Hδ are obviously much larger. The large orbital changes in Hδ may be evidence of the increased importance of the central absorption which appears after phase 0.0. In addition, a smaller contribution to the increased variability may be the blend with He I 4121 Å.

The equivalent widths shown in Figure 8 include contributions from the disk profile as well as the S-wave. An accurate estimate of the relative contributions from these two sources is difficult to make because, over most of the orbit, the S-wave is relatively weak. The most accurate measurements of the equivalent widths of the extracted S-wave can be made between phases 0.35 and 0.55 when the intensity of the S-wave is relatively constant and is at its maximum strength. In Table 4 we list the equivalent widths of the extracted S-wave emission and of the S-wave free-disk emission measured from eight spectra within the phase interval from 0.35 to 0.55. The

TABLE 4

SEPARATED EQUIVALENT WIDTHS

Line	Disk (Å)	S-Wave (Å)
Hβ	35.0 ± 4.4 (1.00)	5.5 ± 0.6 (1.00)
Hγ	18.8 ± 2.9 (0.54)	3.8 ± 1.0 (0.69)
Hδ	16.6 ± 2.7 (0.47)	2.8 ± 0.7 (0.51)

numbers in parenthesis give the line ratios relative to Hβ. From these measurements, we see that the S-wave contributes, at most, 20% of the total equivalent width. There is also a marginal indication that the S-wave Balmer decrement is slightly more shallow than that of the disk emission.

f) *Line Profiles*

The accretion disk emission lines provide a natural diagnostic of the complex physical conditions in which they are formed. In this section we present a phenomenological model of the emission-line profiles which can serve as a guide to additional physical disk models. The characteristics of the observed emission-line profiles depend on several factors: (1) distribution of emission within the disk; (2) inner and outer radii of the disk; (3) turbulent or random motions within the disk; (4) absorption by material in the disk; (5) dependence of rotational velocity on position within the disk; and (6) the instrumental profile. Because the instrumental profile of the CDS is narrow in comparison to the emission-line peaks, it will broaden and smooth the intrinsic profile only slightly. Therefore, in the following analysis, we do not take this effect into account. In addition, our analysis assumes that the average velocity at any point in the disk is equal to its Keplerian velocity about the white dwarf. Furthermore, we do not attempt to account for vertical structure within the disk, nor do we model absorption effects.

While factors (1), (2), and (3) each influence the overall profile, they tend to manifest themselves in distinctly different aspects. The emission distribution dominates the slope of the wings. The size of the outer radius of the disk determines the separation of the peaks, and the inner radius determines the maximum extent of the wings. Finally, the turbulent motions control the width of the peaks. Because half of the separation of the peaks corresponds closely with the rotational velocity at the outer edge of the disk, we can find immediately that the disk in U Gem has an outer radius of 4.5×10^5 km or about $0.4a$, where a is the separation of the two stars. This is a large disk, extending out to about 90% of the Roche lobe radius of the white dwarf. Although our assumption of Keplerian motion becomes inaccurate at such large radii, it is clear that the disk in U Gem is much larger than a zero-viscosity disk (Flannery 1975). In fact, most evidence seems to indicate that accretion disks in all cataclysmic variables are of comparable size to their Roche lobe radii (Robinson 1973; Robinson 1974; Sulkanen, Brasure, and Patterson 1981; Cowley, Hutchings, and Crampton 1981).

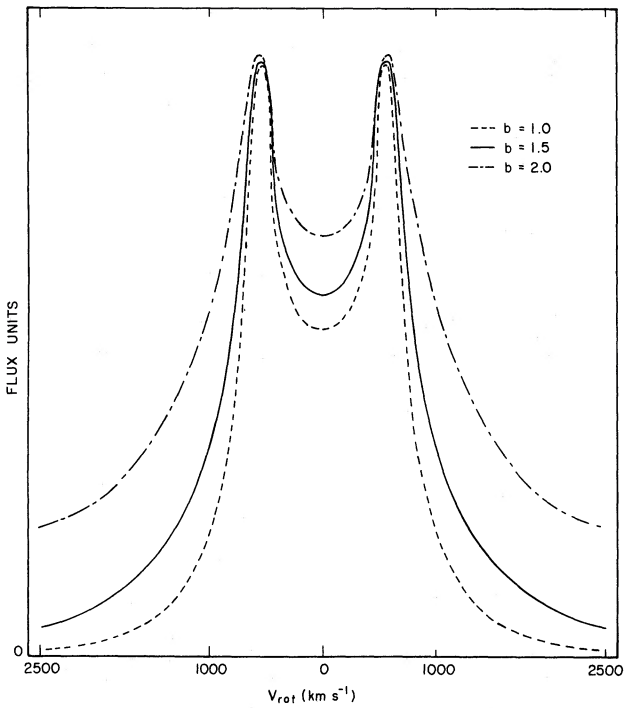

FIG. 9.—Model emission-line profiles. The three profiles illustrate the effect of varying the surface brightness parameter, *b*.

To investigate the effect of the emission distribution on the profile of the emission lines, we have developed a simple disk model in which the surface brightness varies as a function of disk radius:

$$f \propto r^{-b}(\text{flux units cm}^{-2})$$

In the model, the disk is divided into 10,800 segments for which the average surface brightness and projected Keplerian velocity are computed. In each segment, local random and turbulent motions are assumed to form a Gaussian emission-line profile whose characteristic half-width is proportional to the local mean Keplerian velocity. Each point of the final profile is then formed by adding the contributions from all disk segments. Figure 9 shows the effects of varying the surface brightness parameter, b, on the computed line profile. The model with $b = 1.5$ agrees reasonably well with the observed profiles in U Gem. These models were computed assuming that the inner radius of the disk extends down to the surface of the white dwarf, thus producing the maximum possible extent to the wings. However, regardless of the inner radius, models with $b = 2$ produce wings that are much too broad in comparison to the observed profiles in the region $V_{rot} = 1000$ km s^{-1}, and models with $b = 1$ produce wings that are much too narrow. These models also assume that local turbulent velocities are 1.7% of the local Keplerian motion. By increasing the turbulent velocities, the peaks of the emission-line profile can be broadened, and a better match to the observed profile can be obtained. We find that $V_{turb} = 0.12V_{rot}$ produces

profiles which match the observed peak widths reasonably well. Since we have not corrected for instrumental broadening, this value is probably an overestimate. Nevertheless, the modeling clearly shows that turbulent-free motion in the outer portions of the disk of U Gem is unlikely.

Finally, we can adjust the fourth parameter, the inner radius, to terminate the wings at the maximum observed velocity. The maximum observed projected velocity in U Gem is 2500 km s^{-1}, corresponding to a disk radius of about 2×10^4 km. In Figure 10 we show the observed Hβ profile at two orbital phases. In each profile, the S-wave is blended with the blue wing. The solid lines correspond to a model with the following parameters:

$$b = 1.5 ,$$

$$R_{\rm outer} = 4.5 \times 10^5 \text{ km} ,$$

$$R_{\rm inner} = 2.0 \times 10^4 \text{ km} ,$$

$$V_{\rm turb} = 0.12 V_{\rm rot} .$$

Obviously, this model is rather simple and purely mechanical, and, with four free parameters, the good agreement between the observed and computed profiles is not surprising. Nevertheless, the value derived for b is almost independent of the other parameters and is well determined. The concept of an inner disk radius, on the other hand, is rather artificial and probably could be replaced with a model in which b simply decreases near the center of the disk. If the disk has some vertical structure, this could be the result of simple geometrical masking of the central portion of the disk. Furthermore, the maximum extent of the wings, which determines the inner radius, is certainly a function of the signal-to-noise ratio of the data. Additional refinements in the model seem pointless without improvements in our understanding of the physical conditions in the disk which give rise to the observed profiles.

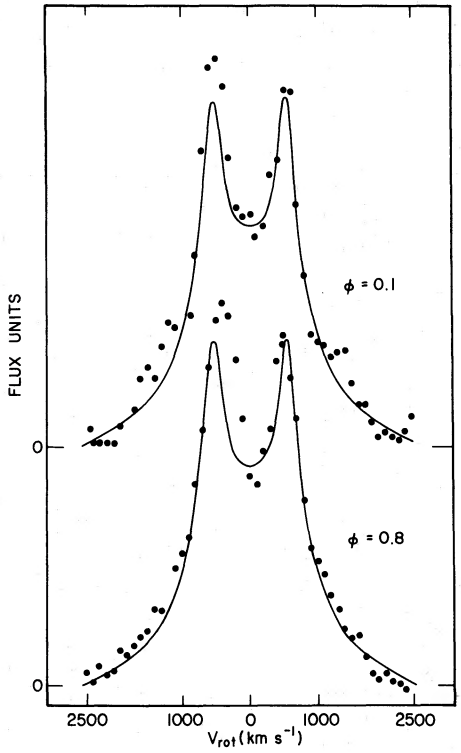

FIG. 10.—Comparison of observed Hβ profiles with model profiles. Observed profiles at orbital phases 0.1 and 0.8 are shown. In each case, the S-wave is blended with the blue wing.

One further comparison can be made between the observed and computed profiles shown in Figure 10. At a projected velocity of about 1000 km s^{-1}, a sudden change of slope occurs in the observed profile so that, at about 1200 km s^{-1}, the observed profile is systematically above the computed profile. Although the difference is particularly apparent in the upper profile in Figure 10, corresponding to orbital phase 0.1, the effect is visible to a greater or lesser extent at all phases shown in Figures 2 and 5. Apparently, but not surprisingly, the surface brightness of the real disk in U Gem follows a more complicated distribution than does our model.

IV. DISCUSSION

a) *Masses and Radii*

Wade (1981) has obtained the first radial-velocity measurements of the secondary star in U Gem using the Na I infrared doublet at 8183 Å and 8194 Å. These measurements permit us, for the first time, to obtain directly the masses of the binary components. Using Wade's (1981) velocity amplitude of 284 ± 15 km s^{-1}, we derive the orbital parameters given in Table 5. The masses and dimensions of the system depend on the inclination which can be estimated from eclipse observations (Smak 1971). However, the eclipse solutions permit a rather wide range of inclinations from about 55° to at least 72°, with the higher end of the range favored slightly. Therefore, we will adopt $i = 67°$ as used by Smak (1976) and Wade (1981). With this inclination we find:

$$M_{\rm wd} = 1.18 \pm 0.15 \, M_\odot ,$$

$$M_{\rm red} = 0.56 \pm 0.06 \, M_\odot .$$

The errors shown here and in Table 2 are internal errors only and do not include the uncertainty in the inclination.

Smak (1976) was able to identify a family of likely masses for U Gem, with the most probable being $M_{\rm wd} = 0.97 \, M_\odot$ and $M_{\rm red} = 0.36 \, M_\odot$. Our derived masses are somewhat higher than those obtained by

TABLE 5

ORBITAL PARAMETERS OF U GEMINORUM ($P = 0^d.176906$, $e = 0$)

Variable	Value
$(M_{\rm wd}/M_{\rm red})$	2.09 ± 0.15
$M_{\rm wd} \sin^3 i \, (M_\odot)$	0.92 ± 0.12
$M_{\rm red} \sin^3 i \, (M_\odot)$	0.44 ± 0.05
$a_{\rm wd} \sin i \, (10^5 \text{ km})$	3.33 ± 0.19
$a_{\rm red} \sin i \, (10^5 \text{ km})$	6.93 ± 0.37

Smak (1976) primarily because of our larger amplitude for the white dwarf velocity variations. It is interesting that our measured amplitude is very similar to Smak's (1976) value before he applied corrections derived from his disk model. In light of our analysis of the emission-line peak velocities, it appears that Smak's (1976) simple model for the accretion disk overestimates the corrections required.

The radius of the secondary star can be obtained by assuming than its radius is equal to the mean radius of its Roche lobe:

$$R_{\rm red} = 0.51 \pm 0.02\ R_\odot\ .$$

Figure 11 shows the relationship of the secondary star mass and radius to that of the empirical zero-age main sequence (ZAMS) estimated by Lacy (1977). The circle corresponds to the values derived in this paper, and the square represents the values found by Smak (1976). The error bars show the 1 σ uncertainty introduced by the radial-velocity measurements, and the arrows indicate the change that would occur for an inclination increase of 8°. Clearly, within the errors of measurement and the uncertainty of the ZAMS, the radius of the secondary star in U Gem is consistent with the mass-radius relation for lower main-sequence stars.

Wade (1979) obtained spectrophotometric observations of the secondary star and classified the spectral type as M4.5. Using a radius $R_{\rm red} = 0.43\ R_\odot$, Wade (1981) found that the implied luminosity is greater than that expected from a main-sequence star of similar spectral type. The discrepancy becomes even larger if the new radius estimate, 0.51 $R_\odot$, is used to estimate the luminosity. Furthermore, the new mass estimate is about twice the expected mass of a main-sequence star of spectral type

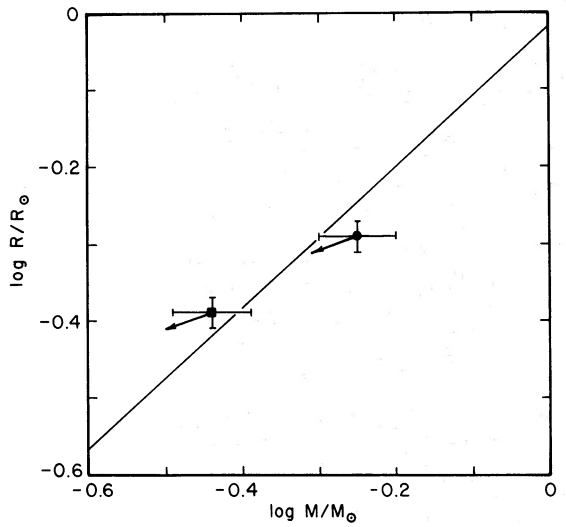

FIG. 11.—The lower main-sequence, mass-radius relationship and the secondary star in U Gem. The circle represents the values derived for the secondary star in this paper. The square represents Smak (1976) derived values. One sigma error bars and the effect of changing the inclination by 8° are shown for each point.

M4.5. Since the secondary star falls on or near the main-sequence, mass-radius relation, the observed spectral type then implies that it is probably underluminous for its mass.

Some investigators have estimated the radius (and mass) of the white dwarf by assuming that the maximum velocity of the emission-line wings corresponds to the Keplerian velocity at the surface of the white dwarf. This procedure clearly fails for U Gem since the observed velocity of only 2500 km s^{-1} predicts a rather large white dwarf with a mass of only 0.5 $M_\odot$. Such a low mass is definitely excluded. If we turn the procedure around, we predict a projected Keplerian velocity of about 5800 km s^{-1}, more than twice the observed value. The implications of the missing wings will be discussed in § IV*b*.

b) *Disk Structure*

Paczynski and Schwarzenberg-Czerny (1980) have suggested that little or no accretion of matter onto the white dwarf takes place between the outbursts of U Gem. Rather, the transferring material builds up in the disk, forming a torus. The dwarf nova eruption is then a result of a disk instability which produces sudden accretion onto the white dwarf with a large release of gravitational potential energy. According to Madej and Paczynski (1977), the inner radius of the torus would be expected to be about 10% of the outer radius. Our modeling of the emission-line profiles tends to support this model. We have shown that the emission surface brightness follows a power law with $b = 1.5$. However, to account for the limited extent of the wings, we find that, in the inner region of the disk, b must, at least, decrease and that the profiles are consistent with no emission at all within a radius of 2×10^4 km. This result must be viewed with caution, of course, because the maximum extent of the wings is inherently a low signal-to-noise measurement, and the rapidly decreasing area at the center of the disk severely limits emission from this region unless the surface brightness is very high.

c) S-*wave*

The S-wave goes through intensity variations which mimic the shape of the Hβ equivalent-width changes shown in Figure 8, but with a greater relative variation. In spite of the problems with determining the true central intensity of the double component discussed in § III*c*, the absence of the S-wave between phase 0.05 and 0.35 appears to be real. There are apparently two contributing mechanisms leading to the absence of the S-wave. The first mechanism is the central absorption which develops as the bright spot comes into prominent view just before the photometric eclipse. The other mechanism is the eclipse by the secondary star of the S-wave–emitting material. The sudden reappearance of the S-wave at nearly maximum strength immediately following the eclipse is particularly dramatic. In fact, higher time-resolution spectroscopy during this phase of the orbit could provide valuable information on the relative posi-

tions of the bright spot and the region of the S-wave emission.

The radial-velocity parameters given in Table 2 for the Hβ and Hγ S-wave show large differences in the amplitude and time of maximum positive velocity. But because of the limited phase coverage in the radial-velocity measurements, the true significance of the differences is not clear. The Hβ measurements, which are more reliable than the Hγ measurements, agree closely with the same measurements made by Smak (1976). However, while our Hγ measurements indicate a higher amplitude and earlier phase, the Smak (1976) Hγ measurements indicate a lower amplitude and later phase. In fact, without additional data, it is not clear how to interpret the differences between Smak's (1976) results and our results since the emitting region was apparently very different during the two sets of observations. The difference is illustrated most dramatically by the He I lines. In the Smak (1976) data, the He I 4471 Å line, though weak, clearly showed the S-wave component. But, in our data, He I 4471 Å is so weak that it is completely invisible on individual spectra. This difference may indicate a difference in mass-transfer rate or disk geometry. In addition, since our observations were made 56 days after an eruption (Mattei 1980) and the Smak (1976) observations were made 36 days after an eruption, the differences may also indicate a slow evolution of the S-wave–emitting region toward lower excitation.

In spite of these differences, our results are qualitatively the same as Smak's (1976), and, interpreted within his model, we reach similar conclusions. The amplitude and phase of the S-wave radial-velocity variations as well as the simultaneous eclipse of the S-wave and the bright spot place the S-wave–emitting region close to the spot. In addition, the narrowness of the S-wave confines the emitting region to a small area, probably in the accretion stream just in front of the spot. However, because, unlike the spot, the S-wave suffers little or no disk obscuration, the emitting region cannot be too close to the spot. Smak's (1976) suggestion of an ionization zone in front of the bright spot appears to be a plausible explanation for the origin of the S-wave.

d) Phase Shifts

Wade (1981) found that spectroscopic conjunction derived from the secondary star's radial-velocity curve occurs 9.4 before the eclipse of the bright spot. This is expected since the bright spot is asymmetrically located on the outer edge of the accretion disk and will be eclipsed a short time after conjunction. However, spectroscopic conjunction derived from our emission-line radial velocities occurs 9.1 ± 3.8 after the time predicted by Wade (1981), implying that spectroscopic conjunction and the eclipse coincide. This is obviously a spurious phase shift associated with the emission lines. In Paper I we found a similar phase shift in SS Cygni. One might wonder if the phases for our emission-line spectra are somehow systematically computed incorrectly. This possibility can be ruled out, however, because the phase shift found in SS Cygni was derived from spectra which showed both the emission spectrum of the disk and the absorption spectrum of the secondary, so that the phases for the two radial-velocity curves were, at least, internally consistent. Instead, the phase shift appears to be a real, systematic, physical effect, present even in the wings of the emission lines. The extent to which the amplitude of the measured velocity variations is affected is not known.

V. CONCLUSION

Smak's (1976) analysis of the masses of U Gem was complicated by the lack of radial-velocity data on the secondary star. He therefore had to depend on a physical model for the S-wave which could allow him to narrow the range of likely masses. The present work, on the other hand, has benefited greatly from Wade (1981) infrared observations of the secondary star, so that we no longer depend on the S-wave, whose parameters are difficult to measure and whose interpretation is very uncertain. Because the present work depends much less on specific models for the disk and S-wave, we expect the masses and radii derived here to be both more reliable and more believable.

As a result of our new measurements of the radial-velocity variations of the emission lines in U Gem, we find that the secondary star is more massive than has previously been thought. Contrary to suggestions by Wade (1981), we also find that the secondary star does lie on the lower main-sequence, mass-radius relationship. This result is important for other studies which use the mass-radius relationship to derive masses in other cataclysmic variables when the orbital inclination is not known.

Our analysis of the emission-line peaks shows that large variations in the separation of the peaks do not occur. In addition, our modeling of the line profiles indicates significant turbulent velocities in the outer portion of the disk. Both of these observations are in conflict with pressure-free disk models in which the motion of the particles in the disk are described solely by the three-body approximation. Furthermore, in a turbulent disk, each point on the observed line profile is the summation from contributions over the entire disk, so that the peak, for instance, cannot be simply related to the motion of particles near the outer edge of the disk. For the model presented in Figure 10, at least one-third of the emission at the peaks originates in regions of the disk whose radii are less than half of the outer radius of the disk.

The extent of the emission-line wings in U Gem is consistent with a model in which material accumulates in the disk between outbursts. However, as we have pointed out, additional observations at all phases of the outburst cycle are needed to investigate the time-dependent behavior of the disk. U Geminorum has been an object of intense study in the past, and it will no doubt continue to be so in the future.

The author wishes to thank Dr. R. E. Nather and Dr. E. L. Robinson whose many helpful discussions have greatly improved the content of this paper. Thanks also goes to Dr. Nather for permission to use his photometric observations of U Gem. Suggestions by B. Paczynski and an anonymous referee were also helpful. This work has been supported by National Science Foundation grants AST 76-23882 and AST 79-06340.

REFERENCES

Cowley, A. P., Hutchings, J. B., and Crampton, D. 1981, *Ap. J.*, **246**, 489.
Flannery, B. 1975, *M.N.R.A.S.*, **170**, 325.
Huang, Su-Shu. 1972, *Ap. J.*, **171**, 549.
Krzeminski, W. 1965, *Ap. J.*, **142**, 1051.
Lacy, Claud H. 1977, *Ap. J. Suppl.*, **34**, 479.
Madej, J., and Paczynski, B. 1977, in *IAU Colloquium 42, The Interaction of Variable Stars with their Environment* (Bamberg: Veroffentlichungen der Remeis-Sternwarte), p. 313.
Mattei, J. 1980, A.A.V.S.O. private communication.
Paczynski, B. 1977, *Ap. J.*, **216**, 822.
Paczynski, B., and Schwarzenberg-Czerny, A. 1980, *Acta Astr.*, **30**, 127.
Robinson, E. L. 1973, *Ap. J.*, **186**, 347.
Robinson, E. L. 1974, *Ap. J.*, **193**, 191.
Smak, J. 1970, *Acta Astr.*, **19**, 155.
———. 1971, *Acta Astr.*, **21**, 15.
———. 1976, *Acta Astr.*, **26**, 277.
Stover, R. J., Robinson, E. L., Nather, R. E., and Montemayor, T. J. 1980, *Ap. J.*, **240**, 597 (Paper I).
Sulkanen, M. E., Brasure, L. W., and Patterson, J. 1981, *Ap. J.*, **244**, 579.
Tull, R. G., Vogt, S. S., and Kelton, P. W. 1979, *Proc. SPIE*, **172**, p. 90.
Wade, R. A. 1979, *A.J.*, **84**, 562.
———. 1981, *Ap. J.*, **246**, 215.
Warner, B., and Nather, R. E. 1971, *M.N.R.A.S.*, **152**, 219.

R. J. Stover: Lick Observatory, N.S. 2, University of California, Santa Cruz, CA 95064